Nova Scientia
Revista de Investigación de la Universidad De La Salle Bajío

Recovery of the response function of a flexible membrane to a volume oscillation using double digital fringe projection technique and frequency filtering

Ubaldo Uribe López [1] / David A. Gutiérrez-Hernández [1] ✉ / Daniel Arturo Olivares Vera [1]
Francisco J. Casillas-Rodríguez [2] / José de Jesús Ibarra-Sánchez [3]

[1] Tecnológico Nacional de México, Instituto Tecnológico de León, División de Estudios de Posgrado e Investigación. León, Guanajuato, México
[2] Universidad de Guadalajara, Centro Universitario De Los Lagos, Departamento de Ciencias Exactas y Tecnología. Lagos de Moreno, Jalisco, México
[3] Universidad Iberoamericana León, Departamento de Ingeniería. León, Guanajuato, México
✉ Correspondence author: david.gutierrez@leon.tecnm.mx

Abstract: this study presents a method to recover the response function of a flexible latex membrane undergoing a dynamic event by volume oscillation using Double Digital Fringe Projection to measure the profile of the surface in a sequence of frames. By applying a frequency filter to the interference pattern, a moiré pattern was obtained. Optical phase retrieval from individual frames was performed using the Isotropic Quadrature Transform Algorithm. This fringe projection technique enables full-field measurements, including edges where other techniques could not perform due to shadows generated by the tilt angle. The procedure was devised as a non-contact system to retrieve the deformation function of a flexible surface, enhancing a valuable aspect of the methodology. The results demonstrate successful recovery of the membrane response function, highlighting the relevance of the method for accurate deformation measurements using a straightforward system. These outcomes provide significant value for the development of precise measurement techniques for flexible structures in engineering applications, such as soft robotics, biomedical devices, and material science.
Keywords: fringe projection; frequency filter; optical phase; flexible membrane; moiré pattern

Resumen: este estudio presenta un método para recuperar la función de respuesta de una membrana de látex flexible sometida a un evento dinámico por oscilación de volumen utilizando Proyección de Franjas Digital Doble para medir el perfil de la superficie en una secuencia de fotogramas. Aplicando un filtro de frecuencia al patrón de interferencia, se obtuvo un patrón muaré. La recuperación de fase óptica de cuadros individuales se realizó utilizando el algoritmo de transformación de cuadratura isotrópica. Esta técnica de proyección de franjas permite realizar mediciones de campo completo, incluidos los bordes donde otras técnicas no podrían realizarse debido a las sombras generadas por el ángulo de inclinación. El procedimiento se ideó como un sistema sin contacto para recuperar la función de deformación de una superficie flexible, mejorando un aspecto valioso de la metodología. Los resultados demuestran una recuperación exitosa de la función de respuesta de la membrana, destacando la relevancia del método para mediciones precisas de la deformación utilizando un sistema sencillo. Estos resultados aportan un valor significativo para el desarrollo de técnicas de medición precisas para estructuras flexibles en aplicaciones de ingeniería, como robótica blanda, dispositivos biomédicos y ciencia de materiales.
Palabras clave: proyección marginal; filtro de frecuencia; fase óptica; membrana flexible; patrón muaré

1. Introduction

There are several optical techniques available to gather surface profile and deformations of an object. These include interferometric digital holography (Múnera, 2013; Wu *et al.*, 2021), structured light using point projection (Cerca *et al.*, 2007) or line projection, fringe projection technique (Zhang, 2012), and a variant called double fringe projection (Sciammarella *et al.,* 2008a; Sciammarella *et al.,* 2008b). The latter-mentioned, technique performs an overlap of two fringe patterns generating a Moiré pattern, which aids in image processing.

Fringe projection finds wide application in biomedicine (Valin *et al.,* 2017), vibration analysis (Verlag, 2002), strain and displacement measurements (Quan *et al.,* 2004), 3D surface reconstruction (Martínez *et al.,* 2005; Soriano-Garcia *et al.,* 2019; Zhang *et al.,* 2021), and other fields, thanks to its features. The technique is easy to calibrate,

affordable components are used, and the fringe patterns for object measurement are digitally generated. This ensures high reproducibility, and the absence of mechanical components minimizes systematic errors.

The aim of this study is to examine the object response to a specific motion. To accurately perform the optical phase recovery, spatial analysis is essential. For individual analysis, it is recommended to utilize methods that rely on a single intensity pattern, such as the Takeda method (Takeda *et al.,* 1982). This method involves Fourier spectrum processing, frequency filtering, centering, and applying a tangential function in the spatial domain. Another approach for phase recovery from a single image is the quadrature transform (Quiroga *et al.,* 2003). This method involves obtaining the quadrature component of the intensity pattern, applying a tangential function for phase retrieval, and then unwrapping it.

Digitalizing physical objects requires thoughtful consideration in the number of captured images. A reduced number of images can accelerate measurements and enhance accuracy by minimizing the influence of surrounding conditions. Hence, it is critical to carefully assess the quantity of registered images and choose a suitable balance between speed and accuracy.

The manuscript is divided into 5 sections. The second section outlines the experimental design, parameters, variables, and system features. Section 3 presents the theoretical description of the techniques used in this study and along with comprehensive details of the experimental setup. Section 4 showcases the conducted simulation and the obtained experimental results. Lastly, section 5 presents the experimental results and the conclusions drawn from the proposed system.

2. Methods, techniques and instruments
2.1. Experimental design description
This study utilizes a systematic procedure, organized into four main stages with multiple steps within each stage. Figure 1 illustrates a visual representative diagram of this procedure, designed to accomplish the objectives.
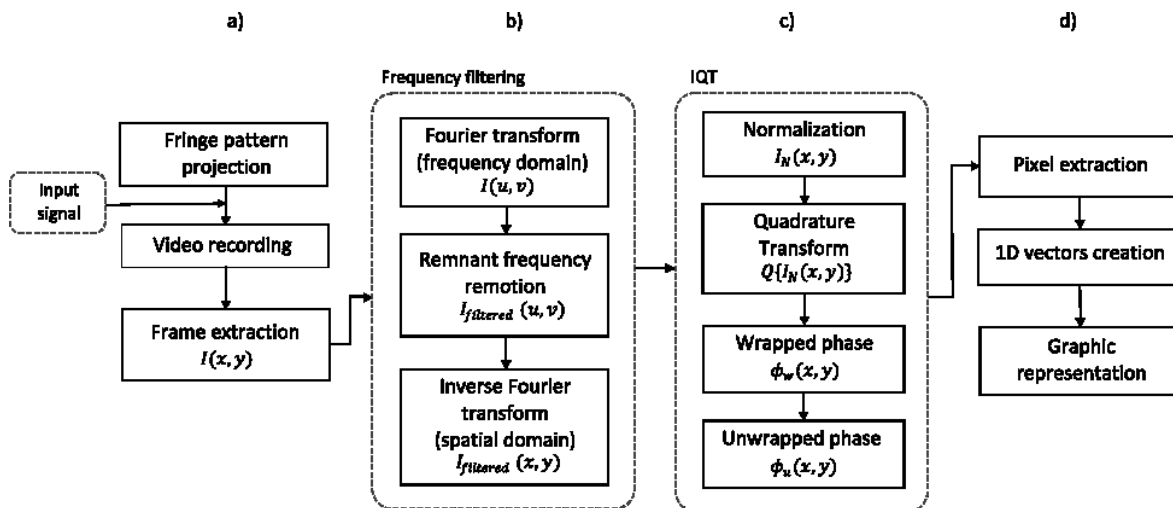
Figure 1. Experimental procedure diagram to retrieve the volume oscillation function of an object subjected to a periodical dynamic event across time.

The experimental process starts with the application of double fringe projection on the object, as depicted in Figure 1a. This step involves generating a periodic event to induce a change in the volume of the object, which then produces an interference pattern recorded using a camera. The resulting images are then separated into individual interference patterns corresponding to distinct event phases.

In the second stage of the procedure (Figure 1b) a frequency filter (Uribe-López *et al.,* 2019a) is employed to process each individual interference pattern through Fourier transform, thereby isolating relevant information, such as zero-frequency component, projected patterns information, and their interference, while eliminating unwanted frequencies. These aspects will be further explained in Section 3. Next, a Gaussian band-pass filter is used to remove unrelated frequencies to the object surface information. Finally, the filtered images go through inverse

Fourier transform, returning them from the frequency domain back to the spatial domain. This process eliminates non-relevant frequencies, resulting in the surface profile information presented as moiré pattern.

The third step of the process (Figure 1c) involves the Isotropic Quadrature Transform (IQT) method for optical phase recovery. The obtained images from the previous step are initially normalized to facilitate phase information retrieval through the quadrature transform. Then, the modulated phase is unwrapped.

To finalize the procedure, the unwrapped phase maps from each frame of the recorded video are employed to extract information from a local cluster of pixels in the top, middle, and bottom regions of the object. This process generates three one-dimensional vectors that graphically represent the output function, as shown in figure 1d.

2.2. Experimental setup and theoretical description.
2.2.1. System parameters and characteristics
This section presents a comprehensive description of the experimental system, which is based on the double digital fringe projection (DDFP) technique in conjunction with the Fourier transform and the IQT method for optical phase acquisition.

Figure 2 illustrates the optical configuration for DDFP system. The imaging system consists of a Garmin VIRB XE camera with a 1/2.3-inch CCD sensor, operating at a video resolution of 1280 x 1024 pixels and a frame rate of 30 frames per second. The illumination setup consisted of two EPSON PowerLite S27 projectors, which provide a luminance of 2700 lumens.

The camera is positioned along the optical axis, centered on the reference plane (x_0, y_0). The projectors are symmetrically arranged on both sides of the camera, with similar angles and distances. They are configured with identical parameters, including contrast, brightness, and focus.

The system alignment involves projecting a black screen with a small white cross from both projectors and aligning them at the center of the reference plane. The inclination and position of the projectors were manually adjusted by projecting binary monochromatic horizontal fringes of equal thickness from one projector at a time, and their positions were adjusted until consistent fringe distances were achieved. A dual HDMI adapter synchronized the projection of the same pattern from both projectors.

2.2.2. Double digital fringe projection
The DDFP technique (Gutierrez-Hernandez *et al.,* 2016; Gutierrez-Hernandez *et al.,* 2015; Uribe-López *et al.,* 2019a; Uribe-López *et al.,* 2019b; Zhang & Yau, 2008) is proposed to acquire surface profile data for a latex membrane. Structured fringes are projected onto the test object using optical devices. Captured pattern images are modulated according to the surface profile of the object (González *et al.,* 2012; Gorthi & Rastogi, 2010; Pérez & Meneses, 2006; Van der Jeught & Dirckx, 2016). These images exhibit an intensity distribution pattern and can be mathematically expressed as equation (1). Digitally processed using fringes analysis techniques (Creath & Wyant, 1992; Malacara, 1990; Servín & Rodríguez-Vera, 1993; Takeda *et al.,* 1982), it obtains phase modulation information. An unwrapping algorithm generates continuous phase distribution maps for each image, facilitating the estimation of displacement maps.

$$I(x,y) = a(x,y) + b(x,y) * cos(2\pi f x + \varphi_0) \qquad (1)$$

In equation (1), the term $a(x,y)$ represents the background light intensity, while $b(x,y)$ denotes the fringe contrast. The parameter f is the spatial frequency of the fringe pattern, along the x-axis, and φ_0 represents the initial phase. By combining the initial phase and frequency terms, the joint phase can be expressed as $\varphi = 2\pi f x + \varphi_0$.

When the fringe pattern is projected onto a non-flat object, it induces deformation in the fringes, which, in turn, leads to modulation in the phase. Therefore, the equation (1) can be modified as follows:

$$I(x,y) = a(x,y) + b(x,y) * cos(\varphi + \Delta\varphi) \qquad (2)$$

The term $\Delta\varphi$ represents the phase change introduced by the object's topography. Equation (2) can be replaced by a single-phase expression including all phases, as shown in equation (3):

$$I(x,y) = a(x,y) + b(x,y) * cos[\phi(x,y)] \qquad (3)$$

The total phase $\phi(x,y)$, and the deformation generated by the test object on the fringes, directly alters this phase. Hence, it is crucial to obtain this phase term to digitize the object in 3D.

To generate a double exposure of fringe patterns, it is necessary to overlap them with the same design of vertical and periodic stripes. Projecting equal frequencies in these patterns creates high-contrast moiré pattern due to the precise alignment of the overlapped stripes, simplifying the phase analysis and resulting in a moiré straightforward process. On the other hand, opting for different frequencies introduces modulation in the moiré pattern due to differences in stripes densities. While this modulation can capture finer surface details, it also adds complexity to the analysis and data processing. Additionally, other parameters such as frequency and angle with opposite sides must be similar. Resulting in this superposition, which is the combination of both patterns, is a Moiré pattern with a different frequency, providing the optical phase information (figure 2).
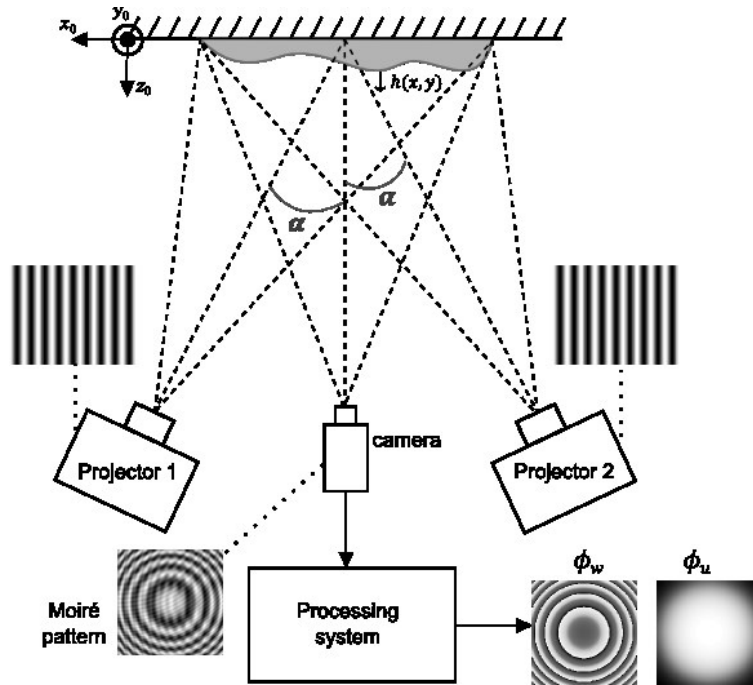
Figure 2. Optical configuration implemented for the DDFP technique. The angle $\boldsymbol{\alpha}$ between the projector and optical axis is shown. The height of the object is represented by $\mathbf{h(x,y)}$, while the wrapped phase is denoted by $\boldsymbol{\phi_w}$ and the unwrapped phase by $\boldsymbol{\phi_u}$.

The angle $\boldsymbol{\alpha}$ directly influences the generation of the moiré pattern. A very small angle, approaching zero, meaning that the projectors are aligned with the optical axis, results in the projected fringes from both sides having minimal or no phase difference, preventing moiré fringes from appearing. An excessively large inclination angle could lead to a Moiré pattern that is overly distorted or dense. Additionally, it may not cover the entirety of the object on the opposite side, thereby increasing occlusion, making analysis difficult, and reducing the measurement area.

In contrast, when the projectors are slightly displaced from the optical axis of the camera, a phase difference is introduced into the projected stripes. This phase difference gives rise to the Moiré pattern when the superimposed stripes combine. The appropriate inclination angle between the projectors and the optical axis of the camera is crucial for creating the necessary phase differences. This, in turn, enables the measurement of the surface topography of the object with a useful and precise Moiré pattern.

Based on equation (3), the intensity of the interference pattern can be described as the superposition of both fringe patterns:

$$I(x,y) = a(x,y) + b_1(x,y) * cos[\phi_1(x,y)] + b_2(x,y) * cos[\phi_2(x,y)] + b_3(x,y) * cos[\phi_3(x,y)] \qquad (4)$$

Uribe et al.

The expression above comprises two phase components for the overlapped fringe patterns and a third phase component that corresponding to the resulting Moiré pattern from their superposition. By expressing the resolved phases, $\phi_n(x,y)$, in terms of their initial values, $\varphi_n(x,y)$, and the surface-induced phase changes, $\Delta\varphi_m(x,y)$, the equation (4) can be reformulated as $\phi_n(x,y) = \varphi_n(x,y) + \Delta\varphi_m(x,y)$, where $n = 1,2,3$, and $m = \alpha,\beta,\gamma$.

$$I(x,y) = a(x,y) + b_1(x,y) * \cos[\varphi_1(x,y) + \Delta\varphi_\alpha(x,y)] + b_2(x,y) * \cos[\varphi_2(x,y) + \Delta\varphi_\beta(x,y)] + b_3(x,y) * \cos[\varphi_3(x,y) + \Delta\varphi_\gamma(x,y)] \qquad (5)$$

The CCD sensor employed for image recording only captures the intensity of the overlapped fringe pattern, without the capability to discern individual frequencies or phases. Consequently, equation (3) defines the final interference pattern that is recorded by the sensor.

The Moiré effect simulation is presented in Figure 3a and 3b, displaying two fringe patterns with circular sinusoidal profiles. The geometric centers of the fringe patterns are positioned on the left and right sides, respectively. Figure 3c presents the overlapped pattern. It showcases the Moiré pattern associated with the horizontal fringes.
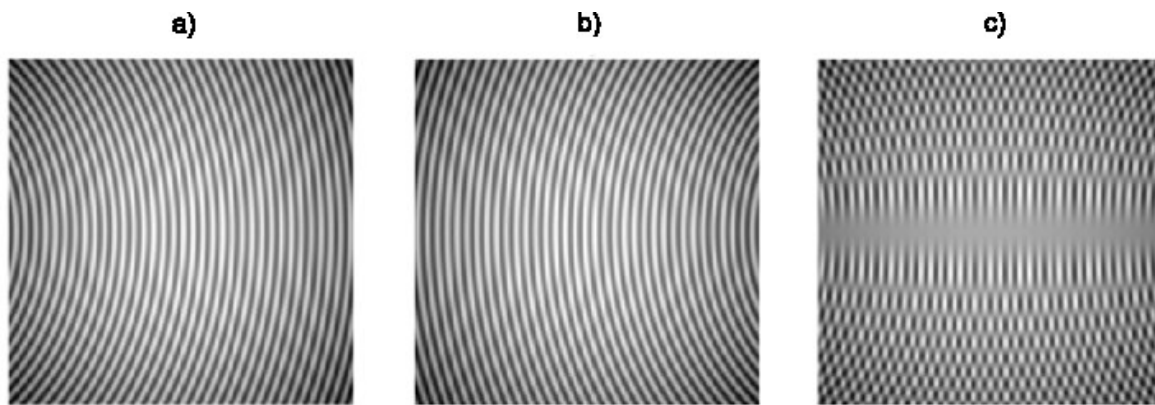
Figure 3. Simulation of Double Fringe Projection using circular sinusoidal profiles for both sides, as shown in a) and b). The resulting Moiré pattern obtained from the overlay of the previous patterns is displayed in c).

2.3. Band-pass frequency filter to retrieve Moiré pattern
In this study, the DDFP technique is used to generate an intensity image incorporating a Moiré interference effect with slightly different frequencies, described by equation (3). However, the resulting pattern may contain undesired fringes with residual frequencies that can compromise the accuracy of the obtained surface profile. To address this issue, a frequency filter can be applied to selectively remove the low and high frequencies that do not contribute to the Moiré pattern. The filtered signal will exclusively contain frequencies present in both patterns, revealing the resultant Moiré pattern upon visualization. A Gaussian distribution band-pass filter is developed for this purpose in the frequency domain (Kreis, 2005; Liu, 2010; Sitni, 2009; Uribe-López *et al.,* 2016). The mathematical analysis involves the modification of equation (3) by substituting the following trigonometric identity.

$$cos(\theta) = \frac{e^{i\theta}+e^{-i\theta}}{2} \qquad (6)$$

Thus, the intensity can be expressed as:

$$I(x,y) = a(x,y) + \frac{1}{2}b(x,y)e^{i\phi(x,y)} + \frac{1}{2}b(x,y)e^{-i\phi(x,y)} \qquad (7)$$

The substitution of the variables $c(x,y)$ and $c^*(x,y)$ for the complex terms in equation (7) results in:

$$c(x,y) = \frac{1}{2}b(x,y)e^{i\phi(x,y)} \qquad (8a)$$

$$c^*(x, y) = \frac{1}{2} b(x, y) e^{-i\phi(x,y)} \qquad \text{(8b)}$$

Upon substituting those variables in equation (7), the resulting expression can be obtained as follows:

$$I(x, y) = a(x, y) + c(x, y) + c^*(x, y) \qquad \text{(9)}$$

These intensity patterns are converted into the frequency domain through the Fourier transform.

$$F\{I(x, y)\} = I(u, v) = A(u, v) + C(u, v) + C^*(u, v) \qquad \text{(10)}$$

The Fourier operator, denoted by $F\{\}$, is applied to the frequency domain coordinates (u, v). The background intensity, represented by $A(u, v)$, corresponds to the zero-frequency term and is centered at coordinates $(0, 0)$. The term $C(u, v)$ contains the required phase information, while $C^*(u, v)$ represents its conjugate.

The mathematical expression for the Gaussian band-pass filter $G(u, v)$ is given by equation (11).

$$G(u, v) = Amp(u, v) * e^{-\left[\left(\frac{u-\mu_u}{\sigma_u}\right)^2 + \left(\frac{v-\mu_v}{\sigma_v}\right)^2\right]} \qquad \text{(11)}$$

The coordinate vectors (u, v) and their unitary amplitude $Amp(u, v)$ are defined. The mean values (μ_u, μ_v) and the standard deviation (σ_u, σ_v) indicate Gaussian distribution center and width. The generated filter is convolved with frequency-domain intensity $I(u, v)$ of the image. The filter parameters are manually set in relation to the structure of the imagen in the frequency domain. The range of standard deviation values is $-1 \leq \sigma_u, \sigma_v \leq 1$, regarding the entirety of the image, with the origin $(0,0)$ being the center of it. Introducing negative values will cause a shift of the Gaussian curve center to the left of the origin for σ_u and downward for σ_v, while positive values will shift it to the right and upwards. The range of values for the mean variables is $0 < \mu_u, \mu_v \leq 1$, altering the size of the Gaussian region, with a value of 1 representing 100% along each axis. Mathematically, by removing the $A(u, v)$ and $C^*(u, v)$ terms, only the $C(u, v)$ term is retained from $I(u, v)$ (Figure 4). Thus, the resulting filtered intensity can be expressed as follows:

$$I(u, v) * G(u, v) = I_{filtered}(u, v) = C(u, v) \qquad \text{(12)}$$
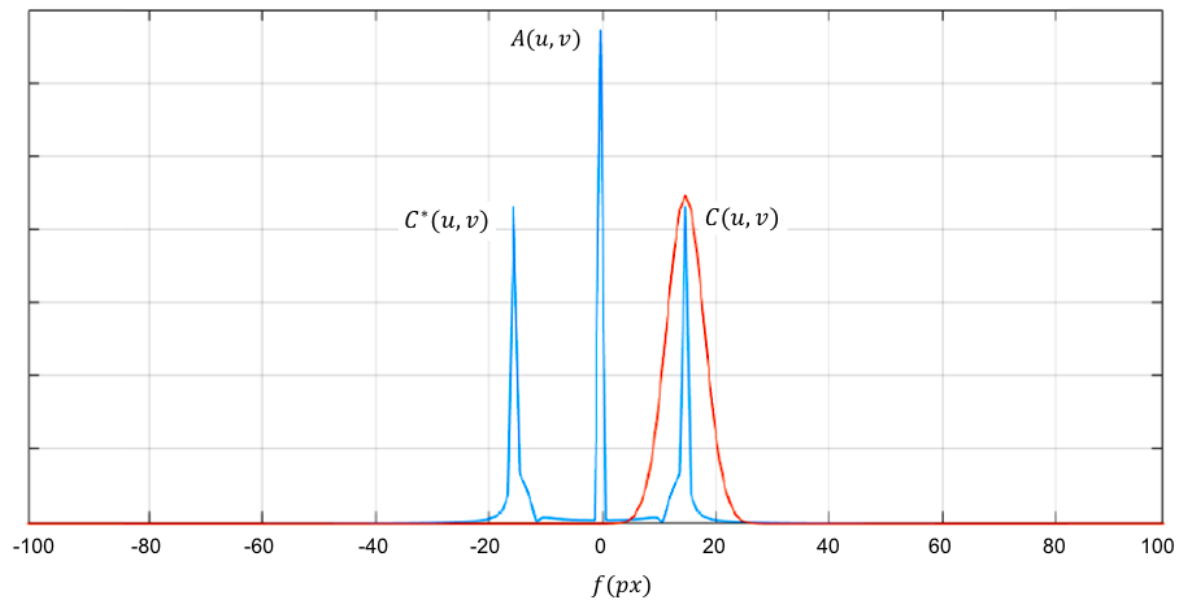
Figure 4. Fourier transform central row from simulated patterns (Figure 3c), represented in blue, along with the Gaussian band-pass filter in red.

Finally, the intensity image is returned to the spatial domain by performing the inverse Fourier transform using the operator $F^{-1}\{\,\}$, as shown in equation (13). The output is a Moiré pattern that has been effectively cleaned by removing the projected fringes.

$$F^{-1}\{I_{filtered}(u,v)\} = I_{filtered}(x,y) = c(x,y) \qquad (13)$$

2.4. Phase retrieval from a single fringe pattern
Spatial analysis is required in phase retrieval for studying objects undergoing continuous deformation in intensity patterns at different time instants during a dynamic event.

The IQT method (Hernández *et al.,* 2018; Larkin *et al.,* 2001; Servin *et al.,* 2003) implemented, enables phase retrieval from a single intensity pattern without requiring a reference pattern. Specifically, the DemIQT function from the XtremeFringe software, developed for Matlab (Quiroga *et al.,* 2015), is employed for this purpose.

The phase retrieval procedure commences with normalizing the intensity pattern, which preserves the Moiré fringe contrast information and phase modulation, yielding $I_N(x,y) = b(x,y)cos[\phi(x,y)]$. Subsequently, the quadrature term is calculated by applying the Hilbert transform of $cos(\alpha)$ using $H\{cos(\alpha)\} = -sin(\alpha)$ for the given pattern, as shown in equation (14).

$$Q\{I_N(x,y)\} = -b(x,y)sin[\phi(x,y)] \qquad (14)$$

The Isotropic quadrature operator, represented by $Q\{\,\}$, is employed to obtain the wrapped phase (ϕ_w) modulated by a tangential function:

$$\phi_w = \arctan\left(\frac{-Q\{I_N\}}{I_N}\right) \qquad (15)$$

The unwrapped phase ϕ_u is obtained using multigrid techniques (Botello *et al.,* 1998; Gräser *et al.,* 2023; Rivera *et al.,* 2015). The demodulated phase of each intensity pattern provides information for analyzing the evolution of the object during the dynamic event.

3. Results
3.1. Simulation and experimental results
This study utilized a flexible latex membrane to examine periodic surface changes. The experimental setup involved electronic, mechanical, and pneumatic components for controlled inflation and deflation. Two projectors illuminated the membrane with the fringe patterns of 0.12 cycles/mm in the reference plane.

To change the membrane's volume, a 0.8 Hz binary signal controlled the air supply, generated by a two-pneumatic valve in series system, using an air compressor, alternating between insertion and ejection. Figure 5 depicts the triangular function representing the air supply compared with the binary signal.
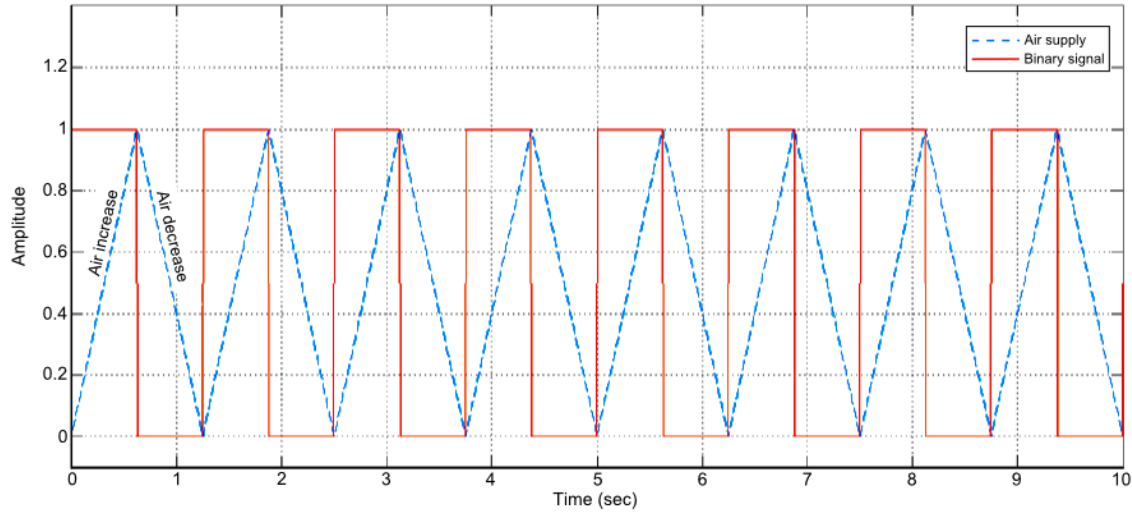
Figure 5. Binary signal function (red) used for the electro-pneumatic system control and the corresponding air supply function (blue).

A video of 26.1 seconds of the membrane in this event is recorded and considering the frames per second rate, there is a total of 783 images for a single processing. Each image is pre-processed by cutting off unnecessary pixels. To analyze the behavior of the membrane, a 26.1-second video was captured, resulting in 783 images. Images were pre-processed to remove unnecessary pixels.

3.2. Simulation

Synthetic circular fringe patterns (see Figure 6a and b) were generated to simulate the membrane deformation using a triangular periodic function for phase modulation $\varphi(x, y)$. The spatial frequency of the fringes varied in each pair of images, increasing, or decreasing according to the modulation function. The images in column c) of Figure 6 show the superposition of pairs of fringe patterns, while the images in column d) depict the resulting Moiré pattern after applying a frequency filter. Finally, columns e) and f) display the wrapped and unwrapped phases, respectively.
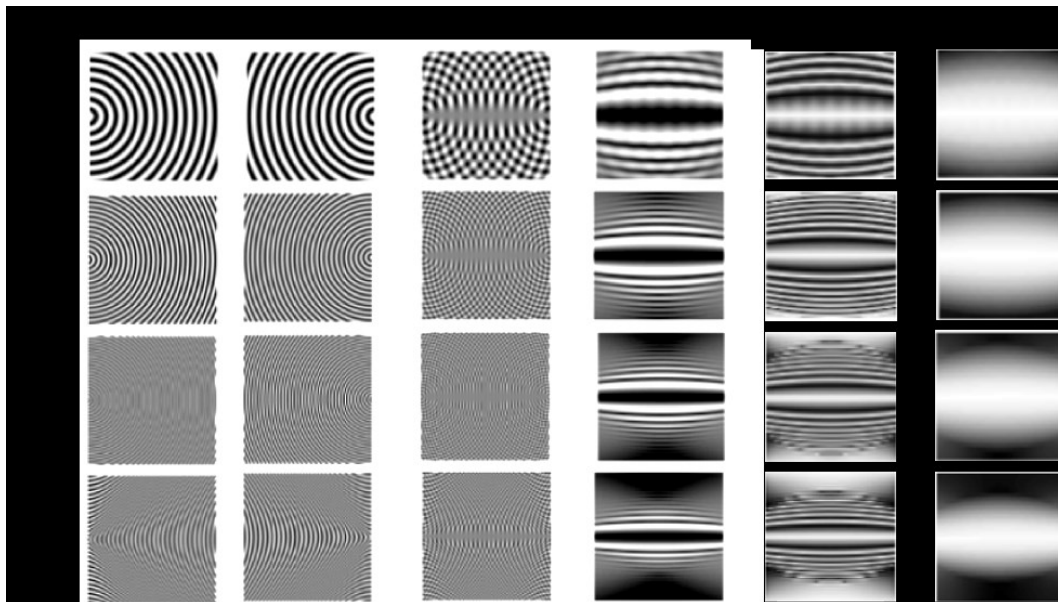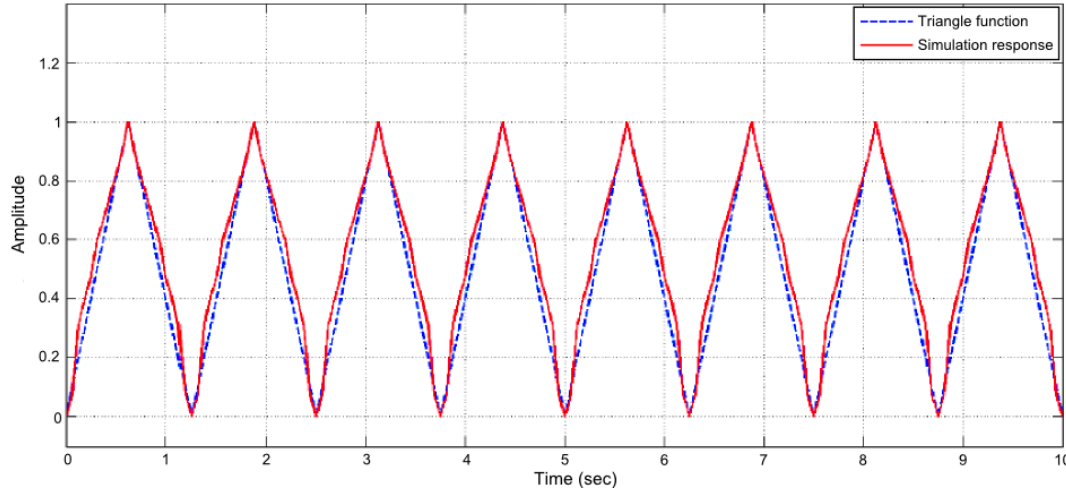

Figure 6. Results obtained from simulating the process using a triangular function as a frequency modulator for the fringes.

Next, information from a pixel section is extracted for every unwrapped phase map, creating a one-dimensional vector to graphically represent the modulation (Figure 1d).

Figure 7 compares the modulation signal of the fringe patterns with the output function extracted from the one-dimensional vector containing information about the frequency and type of function applied to the simulated patterns.


Figure 7. Comparison between the modulation function (blue) and the output function (red) obtained from the simulation process.

3.3. Experimental results

After completing the simulation, the same procedure was performed on a latex membrane, as shown in Figure 8, due to its inherent properties, including high elasticity and capacity to endure considerable deformations without compromising structural integrity. These attributes render the latex membrane an appropriate choice for the investigation, facilitating precise assessment of the flexible surface response to volumetric oscillation.
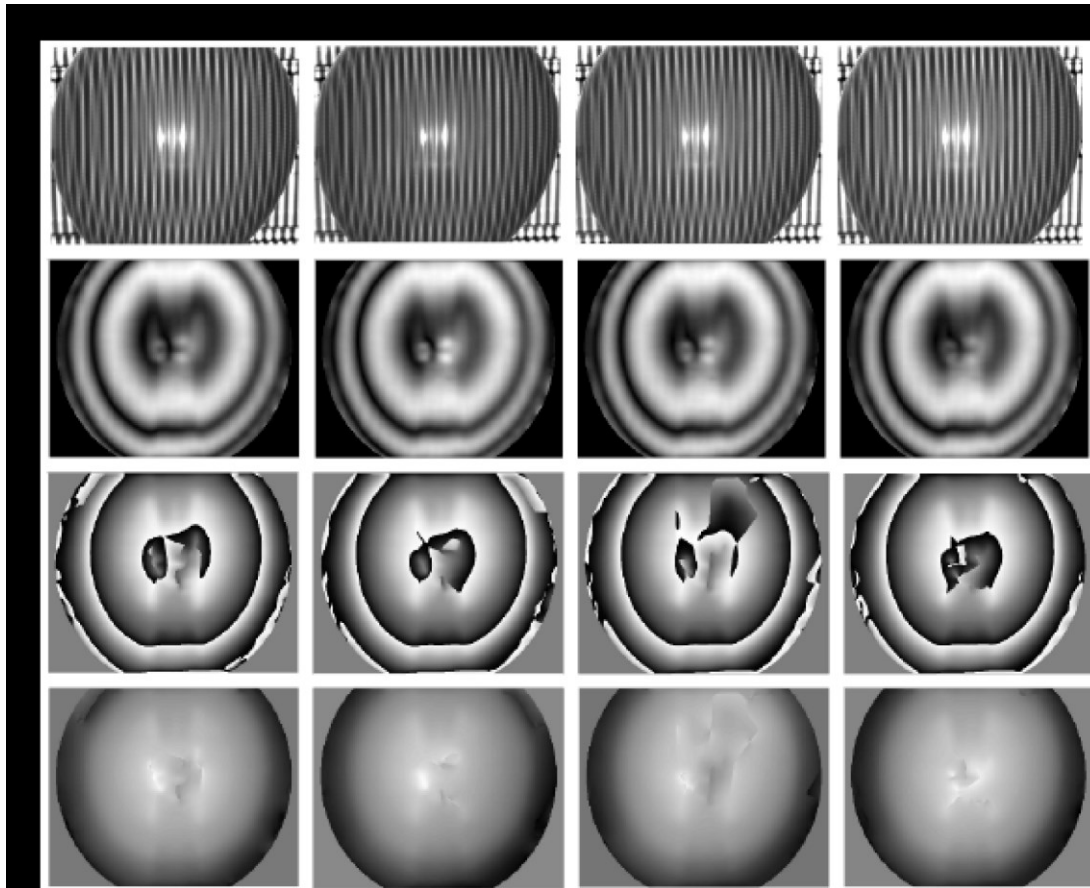
Figure 8. Images representing each step of the procedure outlined in figure 1. 1) Projected fringes interference patterns onto the latex membrane taken from some frames of the video: a) frame 1 (second 0), b) frame 200 (second 6.7), c) frame 400 (second 13.3) y d) frame 600 (second 20); 2) Moiré patterns after applying the frequency filter. 3) Wrapped phases. 4) Unwrapped phases. Three 1D vectors are generated from the extracted pixels in every phase map from the upper (Figure 9a), central (Figure 9b), and lower (Figure 9c) sections of the membrane. These vectors are compared graphically with a triangular function that represents the air supply within the membrane, following the same process used in the simulation.
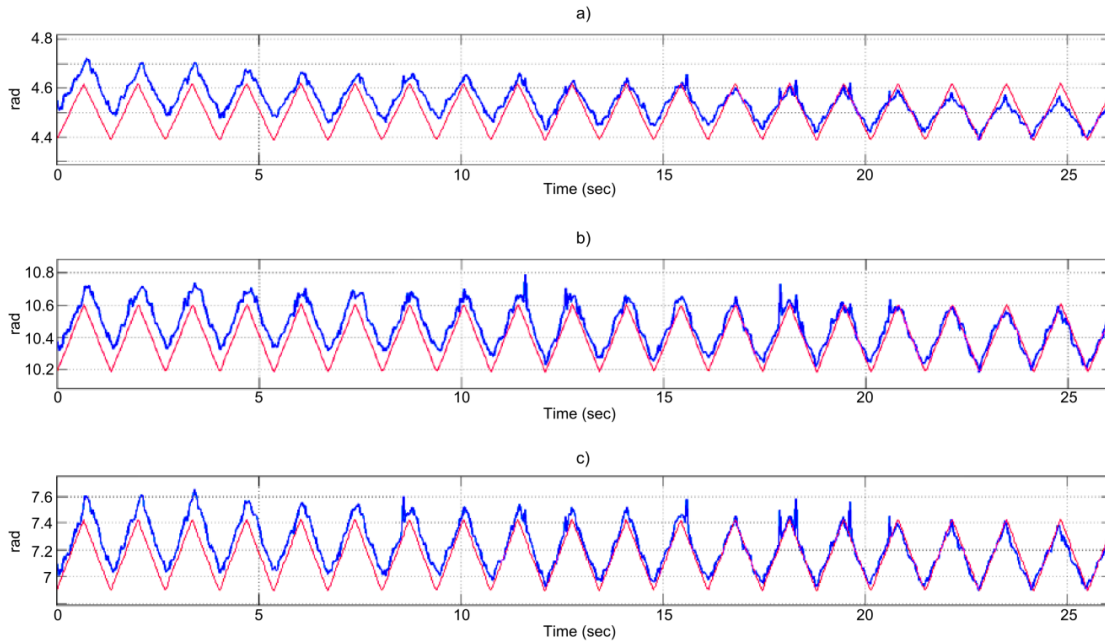
Figure 9. Graphical representation of the volume oscillation in the latex membrane, resulting from the periodic air increase and decrease over 26.1 seconds (blue), compared with a synthetic triangular function (red).

The amplitude of the resulting functions related to the synthetic function varies among the three signals due to their different membrane sections. A reduction in amplitude is observed towards the end of the graph, indicating air attenuation and volume decrease.

The experiment yielded accurate results for the initial function parameters. However, Figure 9 graphically illustrates the error of the overall values related to an ideal simulated triangular function. These discrepancies represent the average absolute difference of all recovered function points in relation to the synthetic function, providing valuable insights ranging from the membrane material characteristics up to the influence of ambient noise. On average, the estimated error in the three signals is 2.7%, as depicted in Figure 10.
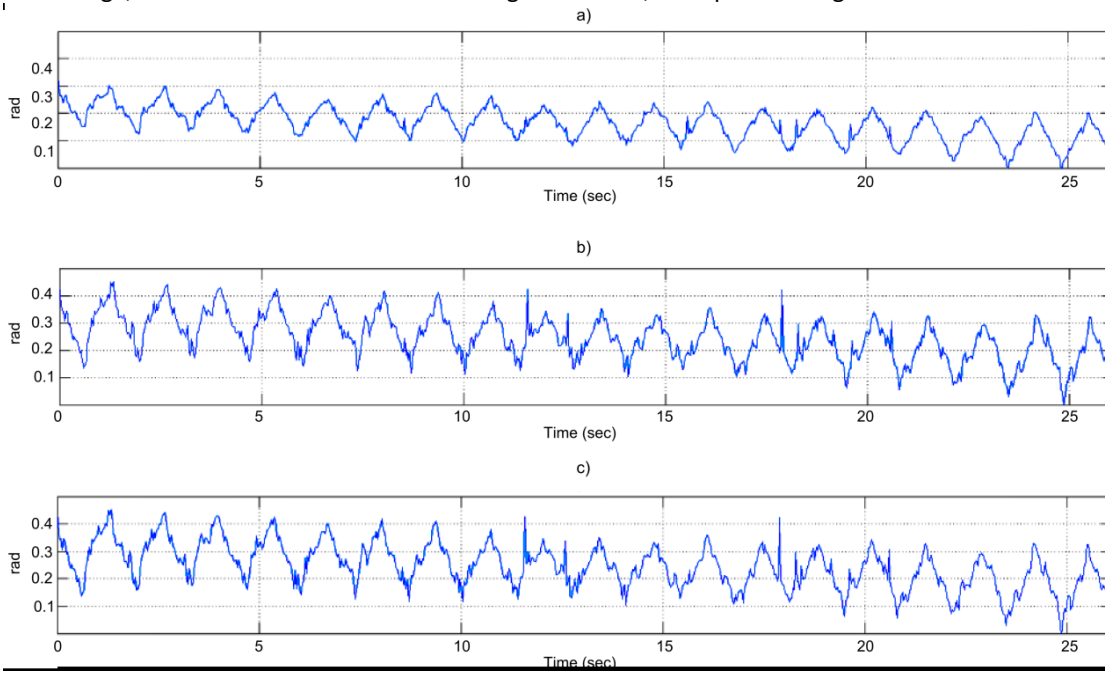
Figure 10. Function errors from the pixel clusters located in the (a) upper, (b) central and (c) lower sections of the membrane, related to a synthetic triangular function.

4. Conclusions

The DDFP technique proves to be a valuable tool for achieving practical and accurate outcomes in this project. It offers precise optical phase estimation for surface profiling, even under challenging conditions such as volume modification. Its straightforward implementation allows for fast measurements, without compromising precision, render it well-suited for engineering applications. The experimental setup facilitates the examination of both dynamic events and static measurements without requiring complex calibration or electronic synchronization.

Previous research has developed measurements for a transient event (Uribe-López *et al.,* 2019b), using a DDFP system to measure the deformation by a volume change without a frequency filter before the phase recovery, resulting in an error of 14%. It was measured using the same methodology as employed to quantify the error in this study, by calculating the average absolute difference between the function acquired through the optical system and a simulated function. In comparison to ideal functions, the implementation of the frequency filter in the current study significantly reduces the phase estimation error of the object by approximately 11.3%, with an average error of 2.7%. Other investigations involved a full-field phase estimation using a frequency filter applied to static objects (Uribe-López *et al.,* 2019a), yielding favorable results and provided a foundation for the development of this work.

The method proposed effectively captures alterations in the volume of the latex membrane through the controlled oscillation of supplied air. It furnishes insights into volume dynamics and membrane properties. The research endeavors to reconstruct the periodic function using frequency and function parameters, rather than surface measurements. The amplitude of the function indicates the adjustable air supply intensity, capable of adapting to different values.

This project provides a foundation for diverse experiments in biometrics, medicine, industry, science, and beyond. It allows for parameter adjustments, encompassing the input signal, the test object, and image processing techniques, such as frequency filtering and phase retrieval. This expands the scope for further research and experimentation.

References

Botello, S., Marroquin, J. L., & Rivera M. (1998) Multigrid algorithms for processing fringe- pattern images. Applied Optics, 37 (32): 7587-7595.

Cerca, M., Barrientos, B., García, J., & Hernández, C., (2007) Obtención del relieve digital mediante proyección de luz estructurada en modelos analógicos de extensión. Boletín de la Sociedad Geológica Mexicana, 59: 101-113.

Creath, K. & Wyant, J. (1992) Optical Shop Testing, John Wiley, New York, pp. 501-599.

González, A., Meneses, J., & León, J. (2012). Proyección de franjas en metrología óptica facial. INGE CUC, 8(1), 191-206.

Gorthi, S. & Rastogi, P. (2010) Fringe Projection Techniques: Whither we are? Optics and Lasers in Engineering. 48(2): 133-140.

Gräser, C., Kienle, D. & Sander, O. (2023). Truncated nonsmooth Newton multigrid for phase-field brittle-fracture problems, with analysis. Computational Mechanics. 1-31. 10.1007/s00466-023-02330-x.

Gutierrez-Hernandez, D., Atondo-Rubio, G., Parra, J., Santiago-Montero, R., Romero, V., Del Valle, J. & Ibarra, I. (2015) Double-digital fringe projection for optical phase retrieval of a single frame. Journal of optoelectronics and advanced materials. 17(9–10), 1248.

Gutierrez-Hernandez, D., Parra, J., Atondo-Rubio, G., Tellez-Quiñones, A. & Del Valle, J. (2016) Fast phase retrieval by temporal phase shifting and double-digital fringe projection. Journal of optoelectronics and advanced materials. 18(9–10), 750.

Hernández, J., De la Rosa, J., Rodríguez, G., Flores, J., Tsonchev, R., Garcia-Torales, G., Alaniz-Lumbreras, D., & González, E., (2018). The 2D Continuous Wavelet Transform: Applications in Fringe Pattern Processing for Optical Measurement Techniques. Wavelet Theory and Its Applications. InTech. DOI: 10.5772/intechopen.74813.

Kreis, T. (2005). Fourier Transform Evaluation. Handbook of Holographic Interferometry: Optical and Digital Methods, John Wiley & Sons Ltd., Bremen, Pp. 256-258.

Larkin, K., Bone, D., & Oldfield, M. (2001) Natural demodulation of two- dimensional fringe patterns. I. General background of the spiral phase quadrature transform. JOSA A, 8: 1862-1870.

Liu, Z., Bu, S., Zhang, C. & Tang, X. (2010) Filter Fourier Coefficients of Shape Projections for 3D Shape Retrieval. International journal on information. 13: 1351-1360.

Malacara, D. (1990) Phase Shifting Interferometry, Revista Mexicana de Física 36(1): 6-22.

Martínez, A., Rayas, J., Vera, R., Flores-Moreno, J., & Aguayo, D. (2005) Técnicas ópticas para el contorneo de superficies tridimensionales. Revista Mexicana de Física, 51(4): 431-436.

Múnera, N. (2013) Interferometría Holográfica Digital en Tiempo Real: Aplicación de la Cuantificación de Deformaciones Mecánicas. M.C. Thesis. Universidad Nacional de Colombia, Facultad de Ciencias. Medellín, Colombia.

Pérez, Z., & Meneses, G., (2006) Aproximación Espacio-Temporal para la medida absoluta de la forma 3D de un objeto por proyección de franjas. Revista de la Sociedad Colombiana de Física. 38(2): 641-644.

Quan, C., Tay, C., Huang, Y., (2004) 3-D deformation measurement using fringe projection and digital image correlation. Optik, 115(4): 164-168.

Quiroga, J., Crespo, D., & Gomez-Pedrero, J., (2015) "XtremeFringe ®: state-of- art software for automatic processing of fringe patterns", Proc. of SPIE, 6616, 66163Y-1- 10.

Quiroga, J., Servin, M., Marroquín, J., & Gomez-Pedrero, J. (2003) isotropic n dimensional quadrature transform and its applications in fringe pattern processing, Proc. SPIE 5144, Optical Measurement Systems for Industrial Inspection III.

Rivera, M., Hernandez-Lopez, F., & Gonzalez, A. (2015) Phase unwrapping by accumulation of residual maps. Optics and Lasers in Engineering, 64: 51-58.

Sciammarella, C. A., Lamberti, L. & Boccaccio, A. (2008a) General model for moiré contouring, part 1: theory. Optical Engineering, 47(3): 033605

Sciammarella, C. A., Lamberti, L., Boccaccio, A., Cosola, E. & Posa, D. (2008b) General model for moiré contouring, part 2: applications, Optical Engineering 47(3):033606

Servín, M. & Rodríguez-Vera, R. (1993) Two-dimensional phase locked loop demodulation of interferograms, Journal of modern optics. 40, 2087-2094.

Servin, M., Quiroga, J. & Marroquín, J. (2003) A general n-dimensional quadrature transform and its applications to interferogram demodulation. JOSA A, 20: 925-934.

Sitni, R. (2009) Four-dimensional measurement by a single-frame structured light method, Applied Optics 48, 3344.

Soriano-Garcia, M., Sevilla-Escoboza, R. & Mora-Gonzalez, M. (2019) Optomechatronics design for mobile fringe patterns with applications on profilometry, IEEE International Autumn Meeting on Power, Electronics and Computing (ROPEC), Ixtapa, Mexico, 1-6.

Takeda, M., Ina, H., & Kobayashi, S. (1982) Fourier-transform method of fringe-pattern analysis for computer-based topography and interferometry. Journal of the Optical Society of America, 72: 156-160.

Uribe-López U., Gutiérrez-Hernández D., Casillas- Rodríguez F., Mora-González M., Muñoz-Maciel J., (2019a) Improvement of fringe quality for phase extraction in double digital fringe projection, Optical Engineering. 58(9): 092605.

Uribe-López, U., et al., Gutierrez-Hernandez, D., Casillas-Rodriguez, F., Tellez-Quiñones, A., Parra-Michel, J., Del Valle-Hernandez, J. & Escobar, M., (2019b) Measurement of transient dynamics on a flexible membrane by double digital fringe projection. Journal of optoelectronics and advanced materials. 21(1–2).

Uribe-López, U., Hernández-Montes, M., and Mendoza-Santoyo, F. (2016) Fully automated digital holographic interferometer for 360 deg contour and displacement measurements, Optical Engineering. 55(12), 121719

Valin, J., Goncalves, E., Vinícius-Soares, P., Milito, G., Palacios-Fernández, F., Roque, G., Ricardo-Pérez, J., & Valin Fernández, M., (2017) Desarrollo del método de Moiré de proyección de franjas para la evaluación de deformaciones en premolares superiores, 20: 22-30.

Van der Jeught, S. & Dirckx, J., (2016). Real-time structured light profilometry: A review. Optics and Lasers in Engineering. Vol 87. (18-31). DOI: 10.1016/j.optlaseng.2016.01.011.

Verlag, F. (2002) "Indications for Optical Shape Measurements," vol. 58, pp. 55–58.

Wu, J., Liu, K., Sui, X., & Cao, L. (2021). High-speed computer-generated holography using an autoencoder-based deep neural network. Optics Letters, 46(12), 2908-2911.

Zhang S. & Yau S.-T. (2008). "Three-dimensional shape measurement using a structured light system with dual cameras," Opt. Eng. 47, 013604–013604.

Zhang, Y., Qu, X., Li, Y. & Zhang, F. (2021). "A Separation Method of Superimposed Gratings in Double-Projector Fringe Projection Profilometry Using a Color Camera". Appl. Sci., 11, 890. https://doi.org/10.3390/app11030890

Zhang, Z. (2012) Review of single-shot 3D shape measurement by phase calculation-based fringe projection techniques, Optics and Lasers in Engineering, 50(8): 1097-1106